Journal of Alloys and Compounds 516 (2012) 201–206

Contents lists available at SciVerse ScienceDirect

Journal of Alloys and Compounds

journal homepage: www.elsevier.com/locate/jallcom

Template-free hydrothermal synthesis of $SrSO_4$:Sm^{3+} microrods and its electron trapping luminescence properties

Jiayue Sun*, Randi Sun, Haiyan Du

School of Science, Beijing Technology and Business University, Beijing 100048, China

ARTICLE INFO

Article history:
Received 26 September 2011
Received in revised form 8 December 2011
Accepted 12 December 2011
Available online 21 December 2011

Keywords:
Chemical synthesis
Crystal growth
Microstructure
Optical properties

ABSTRACT

A hydrothermal process without using any surfactants or templates has been employed to prepare $SrSO_4$ microrods with different crystallographic morphologies. The pH value of the reaction solution is determined to be the key factor in the formation of rod-like morphology. It is found that the length-to-diameter ratio (L/D) of the rod-like $SrSO_4$ crystals increases from 1 to 4 when the pH value increases from 3 to 12. Besides, the effects of hydrothermal reaction time and temperature have been investigated to illustrate the morphological evolution process of $SrSO_4$ crystals, and it is also discussed that the microcrystals formation mechanism of the evolution process.

1. Introduction

In recent years, the fabrication of nano- to microscale inorganic materials with special morphologies and sizes has attracted considerable attention because of their distinctive properties and potential applications compared with bulk materials [1–4]. Thus, the shape control of inorganic micro/nanocrystals is of great interest in the field of materials chemistry. As one of the most important multifunctional inorganic materials, strontium sulfate ($SrSO_4$) plays an important role in various applications including the packing of painting, ceramics polish, cosmetics, electronics, papermaking and so on [5]. Recently, $SrSO_4$ is also considered to be a potential compound used for electron trapping material. Especially, the excellent electron trapping properties of $SrSO_4$ crystals are closely related to their sizes [6,7]. In many reported references [8–12], $SrSO_4$ is mainly prepared by solid-state method and few investigations are concerned with the "soft chemistry" synthesis method. It is widely accepted that the hydrothermal method can control the morphology and particle size of the as-prepared product. In this work, we report the preparation of $SrSO_4$ crystals by the hydrothermal method in mild synthesis conditions without the use of any catalysts, toxic reagent or surfactants and ease of operation. Our work further indicates that the pH value of the reaction solution used for hydrothermal synthesis is the key factor in the formation of rod-like $SrSO_4$ crystals. The morphological evolution process of $SrSO_4$ nanocrystals is proposed to understand the effects of pH values on the morphology of $SrSO_4$ crystals. Besides, it is also discussed that the microcrystals formation mechanism of the evolution process.

2. Experimental

2.1. Hydrothermal synthesis of $SrSO_4$

Analytically pure $Sr(NO_3)_2$, $(NH_4)_2SO_4$, and ethanol are used as the starting materials without further purification. $SmCl_3$ (0.2 M) solution is prepared as stock solution, In a typical synthesis, 2.1163 g analytically pure $Sr(NO_3)_2$ is dissolved in deionized water. Then $(NH_4)_2SO_4$ solution in appropriate quantity and 2 mL $SmCl_3$ are dropped slowly into it with vigorous stirring, resulting in a suspension. The pH value of the resulting colloidal solution is controlled corresponding to the designed experiment group, in which the pH is adjusted by dilute H_2SO_4 or NaOH. Then 30 mL distilled water is added into the mixture under continuous stirring. After 2 h, the mixture is transferred into a 40 mL Teflon-lined stainless steel autoclave. The autoclave is maintained at 200 °C for 20 h and naturally cooled down to room temperature. The as-obtained $SrSO_4$ precipitates are filtered and washed several times with distilled water. Finally $SrSO_4$ microcrystals are obtained after drying at 60 °C for 6 h.

2.2. Characterization

The phase structures of the samples are checked by a SHIMADZU model XRD-6000 X-ray powder diffractometer, using Cu Kα of 1.5405 Å. The particle sizes and morphologies of the as-prepared crystals are measured on a TESCAN VEGA II scanning electron microscope (SEM). Raman spectroscopic measurement is conducted with a PerkinElmer model Flex 400 Raman Spectrometer, using a 785 nm fiber laser with up to 250 mW of power. The above measurements are carried out at ambient and room temperature. The infrared spectra are recorded on a NICOLET model 380 Fourier transform infrared spectrometer, using KBr discs as matrices. Ion exchange or other reactions with KBr have not been observed. The photostimulated luminescence emission spectra (PSL) are observed using a Hitachi F-7000

* Corresponding author. Tel.: +86 10 68985467; fax: +86 10 68985467.
E-mail address: jiayue_sun@126.com (J. Sun).

0925-8388/$ – see front matter © 2011 Published by Elsevier B.V.
doi:10.1016/j.jallcom.2011.12.048

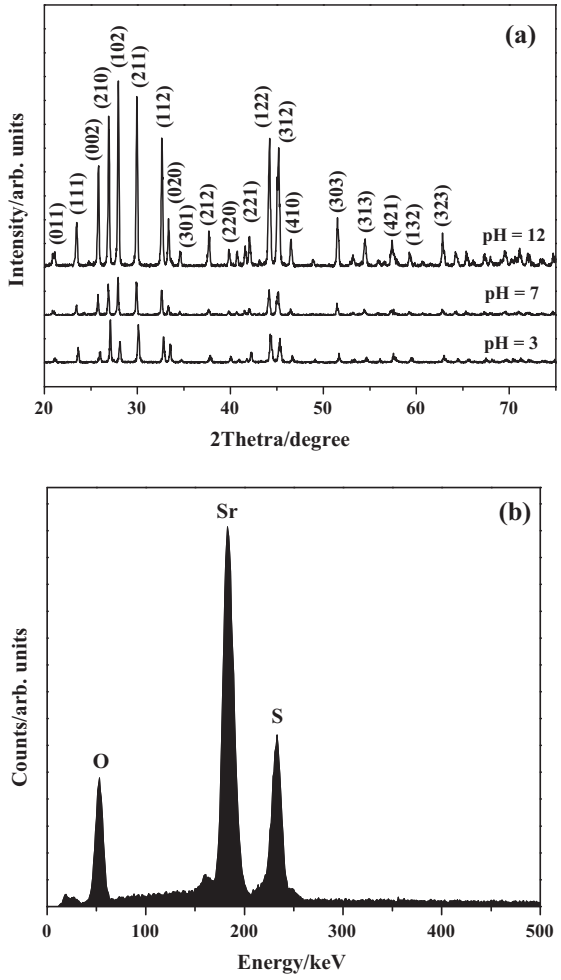

Fig. 1. (a) XRD patterns of $SrSO_4$ crystals obtained at different pH values; (b) EDAX measurement of the $SrSO_4$ samples obtained at pH 12.

spectrophotometer with a 150-W Xe lamp used as the excitation lamp and an external 980 nm semiconductor laser.

3. Results and discussion

3.1. Effect of pH values on the morphology evolution of $SrSO_4$ crystals

The typical XRD patterns of as-prepared $SrSO_4$ crystals obtained at different pH values are shown in Fig. 1(a). Firstly, all the XRD patterns are in agreement with the JCPDS card no. 05-0593 of $SrSO_4$ crystals. Their diffraction peaks can be indexed as the orthorhombic structure crystal. No other diffraction peak appears, indicating that the obtained crystals are all single phase $SrSO_4$. However, careful examination reveals that the intensities of diffraction peaks of the crystals obtained at pH 12 are much stronger than the peaks of the others. This shows that $SrSO_4$ crystals obtained at pH 12 have higher crystallinity degree than the crystals obtained at the other pH values. In order to further confirm the chemical composition of the as-prepared $SrSO_4$ crystals, the analysis of energy dispersive X-ray spectrum (EDAX) gives the chemical composition of the $SrSO_4$ crystals obtained at pH 12 (Fig. 1(b)). A comparison of the relative area under the peaks for Sr, S and O yields an atomic ratio of 1.0:1.0:3.4; the values of S and O is slightly lower than the stoichiometric ratio of 1:4, which is probably due to the hydrolyzation of SO_4^{2-} and the formation of SO_3^{2-}.

Table 1
The FT-IR frequencies of $SrSO_4$ crystal in the range 700–2800 cm^{-1}.

	Vibration modes (cm^{-1})		
	ν_4	ν_1	ν_3
pH 3	612, 644	993	1148
pH 7	613, 645	993	1148
pH 12	604, 644	993	1149

SEM images of the as-prepared crystals obtained by hydrothermal process at different pH values are given in Fig. 2(a–d), and all the crystals show rod-like morphologies with a certain length-to-diameter (L/D) ratio. Clearly it can be observed that the size of the crystal increases with increasing the pH values of the solution. At pH 3, the image reveals that the formed $SrSO_4$ nanorods are uniformly distributed throughout the area of the samples, which are very short and some even are sphere-like with a mean size of around 350 nm, as shown in Fig. 2(a). It should be due to the strongly hydrolyzation of SO_4^{2-} group in the acid condition. Moreover, it is also found that less amount of $SrSO_4$ crystals can be obtained in our controlled experiment at pH 3 compared with the other two conditions because of the strong dissolving behavior of SO_4^{2-} in high acidic condition. Further, at both pH 7 and pH 12, the crystals are rod-like, which indicates that the $SrSO_4$ crystals may grow preferentially along the (2 1 0) direction [13], as shown in the inset of Fig. 2(c). At pH 7, the average length of the nanorods is 2 μm and the width is 600 nm. At pH 12, the crystals grow into large, obvious and perfect $SrSO_4$ microrods, as shown in Fig. 2(c) and (d). It is due to the inhibiting of the hydrolyzation of SO_4^{2-} under the present aqueous basic conditions (pH 12), which leads to larger aggregates [6]. The overall ionic equation for the reaction could be written as:

$$Sr(NO_3)_2 + (NH_4)_2SO_4 \rightarrow SrSO_4 + 2NH_4NO_3$$

$$NH_4^+ + OH^- \rightarrow NH_3{\cdot}H_2O$$

$$SO_4^{2-} + H_2O \rightleftharpoons SO_3^{2-} + 2OH^-$$

$$SO_4^{2-} + 4H^+ \rightleftharpoons SO_3^{2-} + H_2O$$

Based on the experiment, the variation of pH drastically influences the crystallization progress, including crystal nuclei formation and growth, and the morphology of the produced $SrSO_4$ crystals. In the current system, while changing the pH of the reaction system to strong basicity, the aggregation process proceeds at the same time with the formation and growth processes of as-prepared $SrSO_4$ microrods. The result is caused by the increased hydrogen bond interaction between $SrSO_4$ nanorods. Under a low pH value, the formed $SrSO_4$ nuclei adsorb NO^{3-} ions on their surface. However, in basic solution, they adsorb fewer NO^{3-} ions and many more OH^- ions which have hydrogen bond interaction between them [14,15]. As a result, the formed $SrSO_4$ crystals aggregate immediately during the formation and growth processes.

Fig. 3 shows the FT-IR spectra of the $SrSO_4$ crystals at different pH values. Normally, a sulfate contains two S═O and two S—O bonds. Actually, the four S—O bonds are equivalent. The corroborated results put into evidence that at Ph 12, the broad bonding mode around 993 cm^{-1} is attributed to the S—O bonds symmetric stretching mode of the as-prepared $SrSO_4$ crystals. The bands at 604, 644, 993 and 1149 cm^{-1} are characteristic of the sulfate group (S—O) in $SrSO_4$ crystals (Table 1). Upon exposure of the crystals to an acidic condition (pH 3), the ν_1 is weaker than others compared with the $SrSO_4$ crystals obtained at pH 7 and pH 12. It is probably due to lacking of SO_4^{2-}, which has confirmed the results of EDAX analysis under pH 3 condition. The unmarked groups of peaks near 2000 cm^{-1} are overtones. Fig. 4 shows the representative Raman

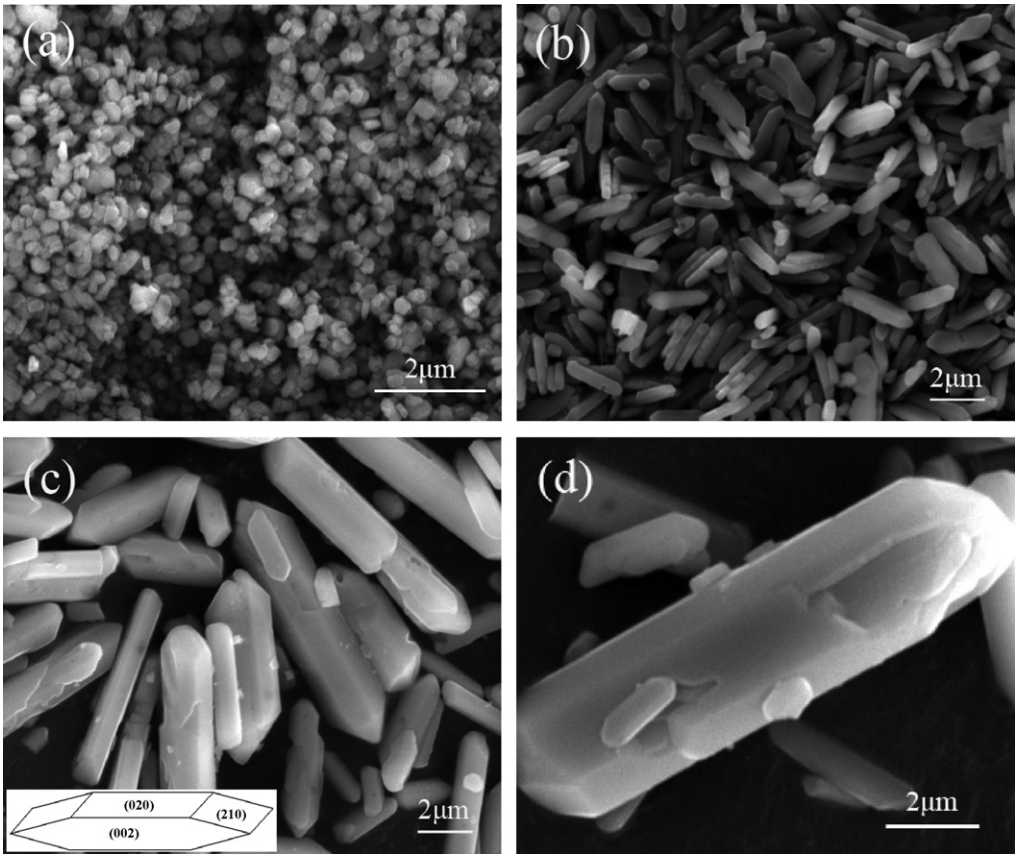

Fig. 2. SEM images of the prepared samples obtained by hydrothermal process (a) at pH 3; (b) at pH 7 and (c) at pH 12 and (d) high magnification of sample in (c).

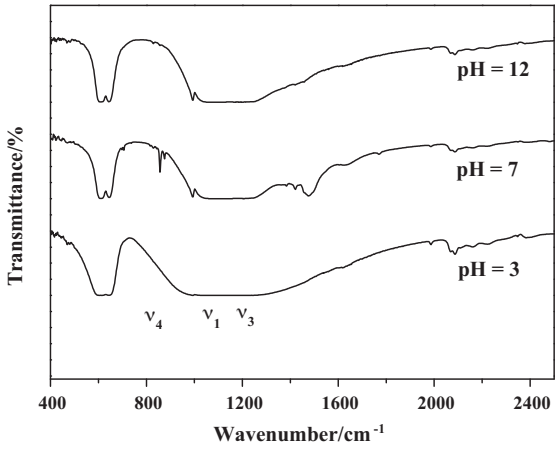

Fig. 3. The FT-IR spectra of the $SrSO_4$ crystals at different pH values.

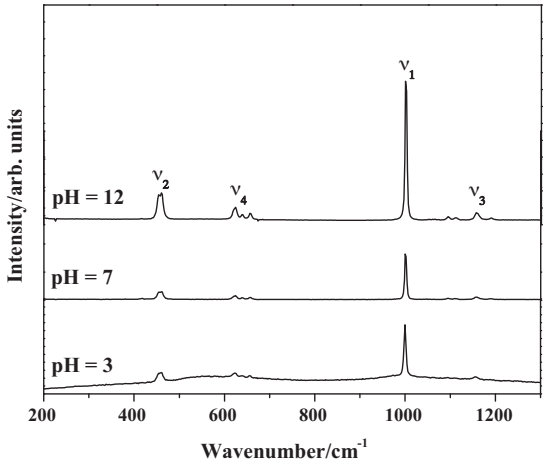

Fig. 4. The Raman spectra of the $SrSO_4$ crystals at different pH values.

spectra of the $SrSO_4$ samples obtained at different pH values. The Raman ν_1 mode (nondegenerate symmetric stretching vibration), ν_2 mode (doubly degenerate deformation), ν_3 mode (triply degenerate stretching vibration), and ν_4 mode (triple bending mode) of $SrSO_4$ crystals with different pH values are observed at ambient conditions (as listed in Table 2), which is in agreement with the report of Chen et al. [16]. The ν_1 mode is the most intense Raman band in the spectra at all pH values. While the pH value

Table 2
The Raman frequencies of the $SrSO_4$ crystal obtained at different pH values.

Specimens	Vibration modes (cm^{-1})			
$SrSO_4$	ν_1	ν_2	ν_3	ν_4
pH 3	1000	454, 460	1060, 1094, 1110, 1156, 1188	624, 640, 656
pH 7	1000	454, 460	1048, 1094, 1110, 1158, 1190	624, 638, 656
pH 12	1000	454, 460	1055, 1093, 1111, 1156, 1190	624, 639, 656

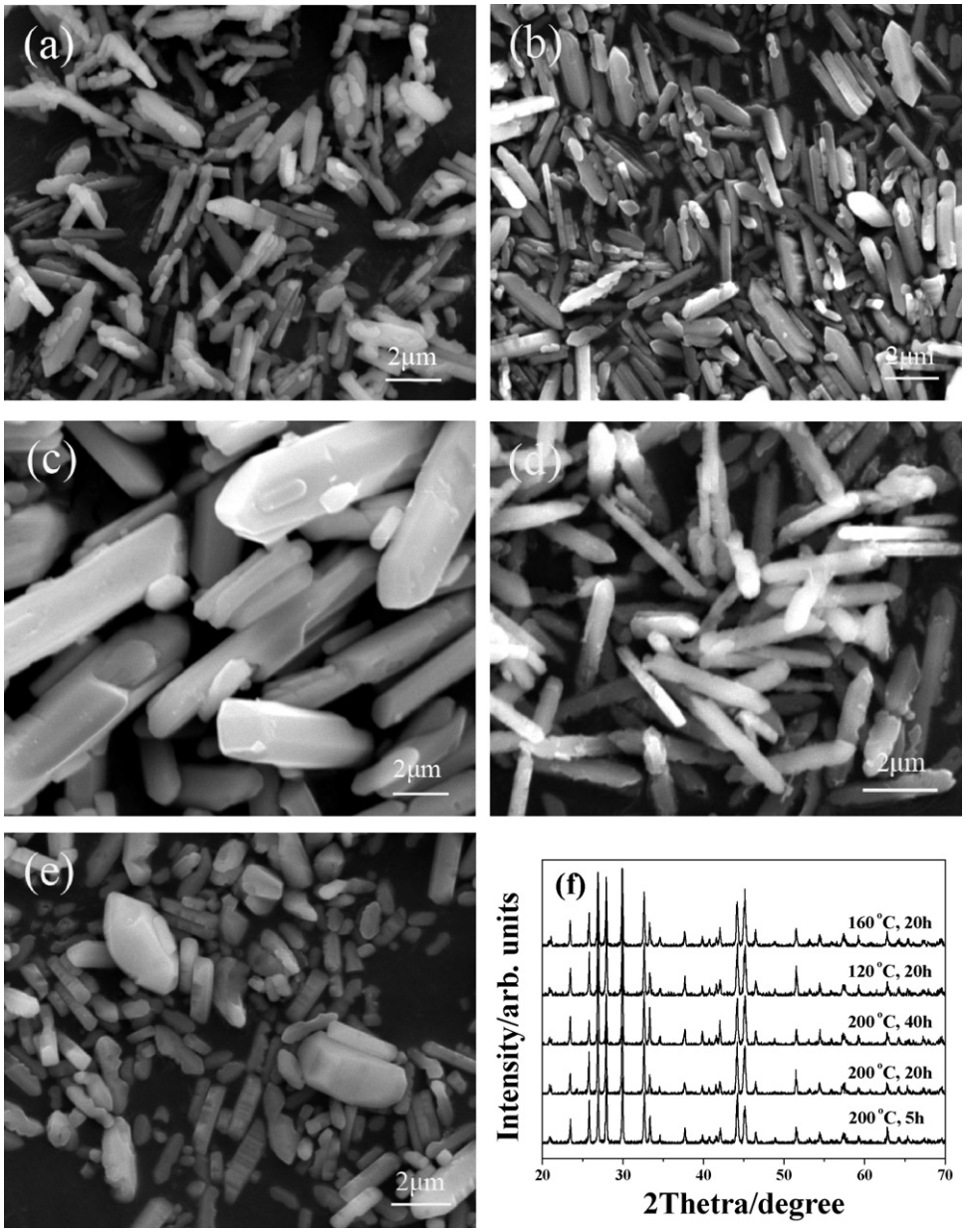

Fig. 5. SEM images of the prepared samples obtained by (a) hydrothermal process at 120 °C for 20 h; (b) hydrothermal process at 160 °C for 20 h; (c) hydrothermal process at 200 °C for 20 h; (d) hydrothermal process at 200 °C for 5 h; (e) hydrothermal process at 200 °C for 40 h; and (f) XRD patterns of $SrSO_4$ crystals obtained at different temperature and reaction time.

decreasing, the crystal size is decreasing. We can observe that the position of the peaks almost have no changes, but all Raman peak intensity decreases, especially the main feature peak at 1000 cm^{-1}, suggesting that the crystal lattices are damaged periodically by a certain degree. It is well-known that, the vibration characteristic peak intensity is weakened because of partly disappeared symmetry. Therefore, it can be found that the line is broadened when the pH value changes from 7 to 3, indicating that the symmetry of the sample is poorer and the degree of disorder is higher.

3.2. *Effect of hydrothermal reaction time and temperature on the morphology evolution of $SrSO_4$ crystals*

In order to further investigate the conditions which can also affect the aggregation process, hydrothermal reaction time and temperature are changed to see the role of hydrogen bond interaction. The pH value of the reaction system is kept at 12, and the reaction conditions for the as-prepared samples are adjusted by controlling different reaction time and temperatures. Fig. 5 shows the SEM images and XRD patterns of the products prepared under different reaction time and temperatures. The results show that $SrSO_4$ nanorods will grow into large microrods with increasing reaction temperatures. When the reaction temperature is kept at 120 °C, the length of the microrods is 4 μm and width is only 250 nm, as shown in Fig. 5(a). At this temperature (120 °C), the nanorods cannot grow into larger ones. When the temperature increases to 160 °C, the agglomeration of $SrSO_4$ microrods is stronger than that under low temperatures and the size of the crystals increases, as shown in Fig. 5(b). Further increasing the reaction temperature to 200 °C, almost all the nanorods assemble into microrods with an average length of 8 μm and width of about 2 μm.

In order to further understand the formation process of the $SrSO_4$ microrods, we have carried out time-dependent experiments, during which samples are collected at different time

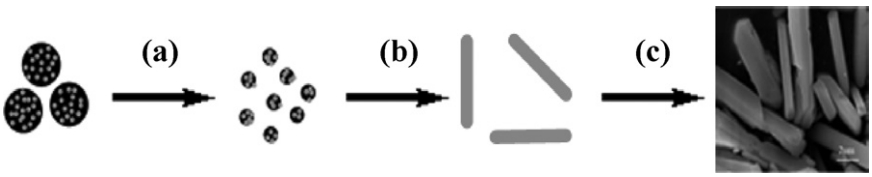

Fig. 6. Schematic illustration of the growth process of $SrSO_4$ microrods, (a) dissolution and crystalline; (b) aggregation; and (c) further growing.

intervals. As shown in Fig. 5(d), when the reaction time is 5 h, the sample is composed of some small nanorods. Almost all $SrSO_4$ crystals grow into microrods with the increasing size after 20 h, as illustrated in Fig. 5(c). The reason is that in a longer period of time the formation and growth of $SrSO_4$ microrods get slowly terminated due to the high activity hydrogen bond interaction, so the agglomeration of $SrSO_4$ microrods is stronger. However, it will induce an inhomogeneity of the sample and both microrods and nanorods are observed when the reaction condition is at 200 °C for 40 h with the width reaching 2 μm while others are still 250 nm, as shown in Fig. 5(e). It is due to an abnormal crystal growth. It is clearly seen from XRD patterns shown in Fig. 5(f) that all samples prepared under different reaction conditions are the pure phase of $SrSO_4$ crystals. Based on the discussion above, crystallinity of $SrSO_4$ crystals is enhanced as a result of hydrothermal processes in strong alkaline solution (pH 12), proper reaction time and temperature.

3.3. Formation mechanism of $SrSO_4$ microcrystals

On the basis of the SEM observations, it can be concluded that the formation of such $SrSO_4$ crystals are achieved via an aggregation process, the happening of which is mainly determined by the hydrogen interaction between $SrSO_4$ crystals, affected by temperature, time and pH values. Any conditional modification, which leads to the changes of the three factors, will greatly affect the diameter and size distribution of the $SrSO_4$ crystals. The possible formation and evolution of such $SrSO_4$ crystals can be shown in Fig. 6. In our study, the formation of $SrSO_4$ crystals is a typical Ostwald ripening process [17–20]. The generation of tiny crystalline nuclei in a supersaturated solution occurs and then follows by crystal growth. The further crystal growth for the formation of $SrSO_4$ crystals is strongly related to the aggregation of the $SrSO_4$ nanocrystals, as shown in Fig. 2(d). At first, primary $SrSO_4$ nanocrystals are formed after the solution becomes supersaturated by adjusting the pH value to 12. Secondly, primary nanocrystals grow into microsized rod-like crystals because OH^- ions are formed on the surface of $SrSO_4$ nuclei, H_3O^+ ions are reduced quickly on their surface and then aggregates into big microrods to lower the surface energy [21–26]. Further, we also propose that the growth of $SrSO_4$ nano/microrods can be caused by several reasons, such as electrostatic, dipolar fields associated with the hydrophobic interactions, specific surface area and van der Waals forces [27].

3.4. Electron trapping luminescence properties of $SrSO_4:Sm^{3+}$ crystals

Trivalent samarium with $4f^5$ configuration has complicated energy levels and various possible transitions between *f* levels. The transitions between these *f* levels are highly selective and of sharp line spectra. Fig. 7 shows the PSL spectra of $SrSO_4:Sm^{3+}$ crystals obtained at different pH values. The $SrSO_4:Sm^{3+}$ crystals are prepumped with short wavelength ultraviolet light to its saturated excited state and subsequently expose to 980 nm laser beams. It can be seen that all the PSL spectra consist of three emission peaks in the visible region at 628, 646, and 668 nm, which can be identified with the $^4G_{5/2}$–^6H_J (J = 5/2, 7/2, and 9/2, respectively) transitions.

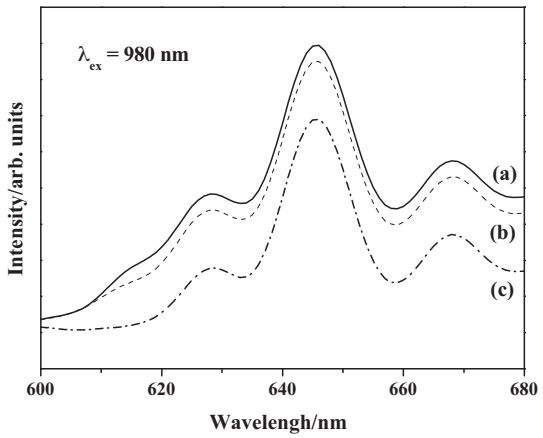

Fig. 7. Photostimulated luminescence spectra of $SrSO_4$ crystals obtained at (a) pH 3; (b) pH 7; and (c) pH 12.

While the size of $SrSO_4:Sm^{3+}$ crystals increases, the PSL intensity decreases, which is in agreement with the early studies of ours [6,7]. The fine PSL property indicates that they have excellent optical storage property.

It is similar to Fig. 7 that the PL spectra of $SrSO_4:Sm^{3+}$ crystals obtained at different pH values consist of three emission peaks, as shown in Fig. 8. Clearly, three emission peaks can be identified with the $^4G_{5/2}$–^6H_J (J = 5/2, 7/2, and 9/2, respectively) transitions. Compared with the PSL spectra, blue shift can be observed in the PL spectra. The three emission peaks are in the visible region at 560, 596, and 641 nm, respectively. According to Figs. 7 and 8, all the peaks in the PSL and PL spectra of $SrSO_4:Sm^{3+}$ can be assigned to the transitions of Sm^{3+} ions, while no peak is assigned to the transition of Sm^{2+} ions [28–32]. It can be observed that the peak intensity of samples decreases with increasing the size, which is similar to the results by Samaele, et al. [33].

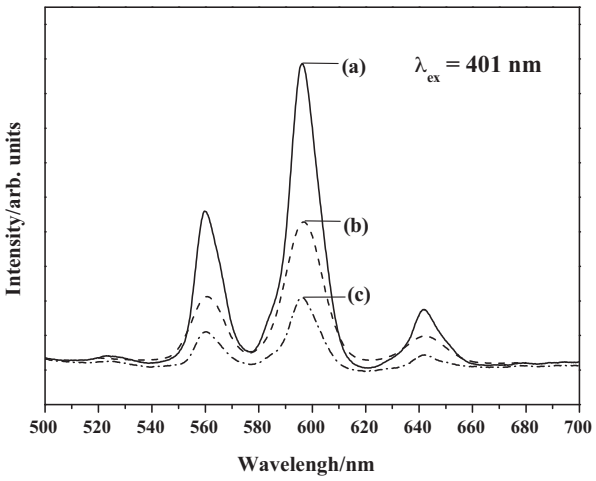

Fig. 8. Photoluminescence spectra of $SrSO_4$ crystals obtained at (a) pH 3; (b) pH 7; and (c) pH 12.

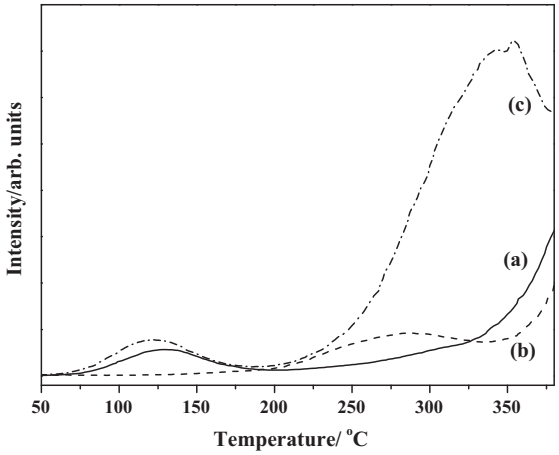

Fig. 9. Thermoluminescence glow curve of crystals obtained at (a) pH 3; (b) pH 7; and (c) pH 12.

Fig. 9 shows characteristic thermal luminescence (TL) spectra of $SrSO_4$:Sm^{3+} crystals obtained at different pH values. As is evident, there are two peaks around 124 and 354 °C in the TL spectrum of microcrystals obtained at pH 12. The peak position of the microcrystals shifts right compared with the spectrum of nanocrystals (pH 3 and pH 7). To verify further, the functions have been modified by Eq. (1) given by Randall and Wilkins [34]. They assumes that (i) spectrum peaks corresponding to different trapping levels do not overlap, (ii) no retrapping occurs in the processes of TL emission and (iii) the life time (z) for recombination is so small that $dn/dt \ll z$ where n is the concentration of the electrons in the conduction band. Further, assuming the frequency factor $s = 109\,s^{-1}$, they derives a simple equation for trap depth as follows.

$$E = 21kT_m \quad (1)$$

where k is the Boltzmann's constant and T_m is the temperature maximum. According to the equation, the trap depth (E) increases with T_m increasing. Therefore, it can be concluded that the trap depth in microcrystals is much deeper than in nanocrystals and more electron transition energy is needed by thermal process with increasing the trap depth.

4. Conclusions

In summary, we have demonstrated a template-free hydrothermal method to synthesize $SrSO_4$ microrods by the reaction between $Sr(NO_3)_2$ and $(NH_4)_2SO_4$. The pH value, reaction temperature and time appear to be important parameters for the morphology evolution of $SrSO_4$ crystals. By adjusting different experimental conditions, $SrSO_4$ microcrystals with different diameters and size distribution are obtained. Especially, the crystallographic morphology of $SrSO_4$ crystals mainly depends on the pH value of the reaction solution. The morphology of $SrSO_4$ crystals synthesized at pH 3 has a short L/D and some of them are even sphere-like with a diameter of 350 nm. However, $SrSO_4$ crystals obtained at pH 7 are rod-like with a length of 2 μm and a width of 600 nm. At pH 12, the crystals grow into microrods with a length of 8 μm and a width of 2 μm. The optical spectra show that the as-prepared $SrSO_4$ crystals under pH 12 condition have high crystalline and excellent luminescence properties related with electron trapping.

Acknowledgements

This work is supported by the National Natural Science Foundations of China (Nos. 20876002 and 20976002), Natural Science Foundation of Beijing (No. 2122012), and Funding Project for Academic Human Resources Development in Institutions of Higher Learning Under the Jurisdiction of Beijing Municipality.

References

[1] J.L. Ning, D. Wang, J. Alloys Compd. (2011), doi:10.1016/j.jallcom.2011.11.075.
[2] M. Zahedifar, M. Mehrabi, Nucl. Instrum. Methods B 268 (2010) 3517–3522.
[3] G. Li, C. Li, H. Tang, K. Cao, J. Chen, F. Wang, Y. Jin, J. Alloys Compd. 501 (2010) 275–281.
[4] S. Tang, M.L. Huang, J.L. Wang, F.D. Yu, G.L. Shang, J.H. Wu, J. Alloys Compd. (2011), doi:10.1016/j.jallcom.2011.10.093.
[5] Y.F. Li, J.H. Ouyang, Y. Zhou, X.S. Liang, J.Y. Zhong, Mater. Lett. 62 (2008) 4417–4420.
[6] J.Y. Sun, R.D. Sun, Z.G. Xia, H.Y. Du, CrystEngComm (2011), doi:10.1039/c1ce06140b.
[7] J.Y. Sun, R.D. Sun, H.Y. Du, J. Funct. Mater. 8 (2011) 1536–1542.
[8] A. Choubey, S.K. Sharma, S.P. Lochab, D. Kanjilal, J. Phys. Chem. Solids 72 (2011) 136–143.
[9] J. Manam, S. Das, Opt. Mater. 31 (2009) 1231–1241.
[10] W.S. Wang, L. Zhen, C.Y. Xu, W.Z. Shao, CrystEngComm 13 (2011) 620–625.
[11] T. Mikami, T. Sakuma, I. Hirasawa, Chem. Eng. Res. Des. 88 (2010) 1200–1205.
[12] Y.F. Li, J.H. Ouyang, Y. Zhou, X.S. Liang, T. Murakami, S. Sasaki, J. Crystal Growth 312 (2010) 1886–1890.
[13] Y.F. Li, J.H. Ouyang, Y. Zhou, X.S. Liang, J.Y. Zhong, Mater. Lett. 62 (2008) 4417–4420.
[14] R.J.H. Grisel, P.J. Kooyman, B.E. Nieuwenhuys, J. Catal. 191 (2000) 430–437.
[15] D. Yin, L. Qin, J. Liu, C. Li, Y. Jin, J. Mol. Catal. A: Chem. 240 (2005) 40–48.
[16] Y.H. Chen, S.C. Yu, E. Huang, P.L. Lee, Physica B 405 (2010) 4386–4388.
[17] W.S. Wang, L. Zhen, C.Y. Xu, L. Yang, W.Z. Shao, J. Phys. Chem. C 112 (2008) 19390–19398.
[18] T.K.N. Hoang, V.B. La, L. Deriemaeker, R. Finsy, Langmuir 17 (2001) 5166–5168.
[19] A.M. Djerdjev, J.K. Beattie, Langmuir 24 (2008) 7711–7717.
[20] P. Dagtepe, V. Chikan, J. Phys. Chem. C 114 (2010) 16263–16269.
[21] J. Zhang, Z. Lin, Y. Lan, G. Ren, D. Chen, F. Huang, M. Hong, J. Am. Chem. Soc. 128 (2006) 12981–12987.
[22] H. Zeng, P. Liu, W. Cai, X. Cao, S. Yang, Crystal Growth Des. 7 (2007) 1092–1097.
[23] M.A.V. Huis, L.T. Kunneman, K. Overgaag, Q. Xu, G. Pandraud, H.W. Zandbergen, D.L. Vanmaekelbergh, Nano Lett. 8 (2008) 3959–3963.
[24] M. Godinho, C. Ribeiro, E. Longo, E.R. Leite, Crystal Growth Des. 8 (2007) 384–386.
[25] X. Wang, J.B. Xu, N. Ke, J. Yu, J. Wang, Q. Li, H.C. Ong, R. Zhang, Appl. Phys. Lett. 88 (2006) 223108.
[26] Z. Zhang, H. Sun, X. Shao, D. Li, H. Yu, M. Han, Adv. Mater. 17 (2005) 42–47.
[27] L. Xu, Y.-S. Ding, C.-H. Chen, L. Zhao, C. Rimkus, R. Joesten, S.L. Suib, Chem. Mater. 20 (2008) 308–316.
[28] S. Sakirzanovas, A. Katelnikovas, D. Dutczak, A. Kareiva, T. Jüstel, J. Lumin. 131 (2011) 2255–2262.
[29] P. Mikhail, K. Ramseyer, G. Frei, F. Budde, J. Hulliger, Opt. Commun. 188 (2001) 111–117.
[30] B.F. Lei, S.Q. Manb, Y.L. Liu, S. Yue, Mater. Chem. Phys. 124 (2010) 912–915.
[31] P. Mikhaila, J. Hulligera, K. Ramseyerb, Solid State Commun. 112 (1999) 483–488.
[32] R.L. Dixon, K.E. Ekstrand, J. Lumin. 8 (1974) 383–390.
[33] N. Samaele, P. Amornpitoksuk, S. Suwanboon, Powder Technol. 203 (2010) 243–247.
[34] R. Randall, M.H.F. Wilkins, Proc. Royal. Soc. A184 (1945) 336–390.